This article has been accepted for inclusion in a future issue of this journal. Content is final as presented, with the exception of pagination.

Kinetically Stabilized Hafnia Ferroelectric of Al-Doped HfO_2 Film by Fast Ramping and Fast Cooling Process

Lingwei Zhang, Giuk Kim, *Graduate Student Member, IEEE*, Sangho Lee, *Graduate Student Member, IEEE*, Hunbeom Shin, *Graduate Student Member, IEEE*, Youngjin Lim, Kang Kim, Il-Kwon Oh, Sang-Hee Ko Park, Jinho Ahn, and Sanghun Jeon, *Senior Member, IEEE*

***Abstract*— Hafnia-based ferroelectrics (FEs) can be stabilized via careful engineering, both kinetically and thermodynamically. Especially, the fast cooling process has been regarded as an efficient approach for kinetically maximizing the phase transition to the orthorhombic (*o*-) phase from the tetragonal (*t*-) phase, which stabilizes thermodynamically during crystallization annealing. However, accurately controlling the cooling period for fast cooling procedures is challenging, resulting in unreliable and nonreproducible outcomes and interpretation. Thus, until now, comprehending its effects has mainly relied on modeling efforts in the field of material science. Here, for the first time, we experimentally validate the fast-cooling effect with Al:HfO_2 FEs, based on the novel equipment ensuring both reliability and reproducibility. In addition, it enabled us to investigate the impact of the fast cooling process on the phase, domain size, and interface quality of FEs through various electrical analyses. The fast cooling technique facilitates the transition from the *t*-phase to the desired *o*-phase, inducing significantly higher remanent polarization values of $2P_r$ (35.31 μC/cm^2) and improved subloop characteristics. In contrast, slow cooling ($2P_r$ of 9.50 μC/cm^2) leads to poor subloop properties. Given that a fast cooling procedure is useful for stabilizing the FE *o*-phase in thin films, we believe that our reliable annealing procedure and significant experimental findings can provide a foundation for future studies in hafnia FE material and memory devices.**

***Index Terms*— Al-doped HfO_2, annealing, fast ramping fast cooling (FRFC), ferroelectric (FE), metal–FE–metal (MFM) capacitors.**

Received 4 September 2024; accepted 23 September 2024. This work was supported in part by K-CHIPS (Korea Collaborative and High-tech Initiative for Prospective Semiconductor Research) under Grant 1415187675, Grant 00235655, and Grant 23006-15TC; in part by the Ministry of Trade, Industry and Energy (MOTIE, Korea) under Grant 1415187390, Grant 00231985, and Grant 23005-30FC; and in part by the National Research Foundation of Korea (NRF) grant funded by the Korea Government (Ministry of Science and ICT) under Grant RS-2023-00260527. The review of this article was arranged by Editor P.-Y. Du. *(Lingwei Zhang and Giuk Kim contributed equally to this work.) (Corresponding authors: Jinho Ahn; Sanghun Jeon.)*

Lingwei Zhang, Giuk Kim, Sangho Lee, Hunbeom Shin, and Sanghun Jeon are with the School of Electrical Engineering, Korea Advanced Institute of Science and Technology (KAIST), Daejeon 34141, South Korea (e-mail: jeonsh@kaist.ac.kr).

Youngjin Lim is with the Department of Intelligence Semiconductor Engineering, Ajou University, Suwon 16499, South Korea.

Kang Kim and Sang-Hee Ko Park are with the School of Materials Science and Engineering, South Korea Advanced Institute of Science and Technology (KAIST), Daejeon 34141, South Korea.

Il-Kwon Oh is with the Department of Electrical and Computer Engineering and Department of Intelligence Semiconductor Engineering, Ajou University, Suwon 16499, South Korea.

Jinho Ahn is with the Division of Materials Science and Engineering, Hanyang University, Seoul 04763, Republic of Korea (e-mail: jhahn@hanyang.ac.kr).

Color versions of one or more figures in this article are available at https://doi.org/10.1109/TED.2024.3475308.

Digital Object Identifier 10.1109/TED.2024.3475308

I. Introduction

HAFNIA-BASED materials with a variety of dopants, including Zr, Sr, Al, Si, La, Gd, and Y, have drawn notable attention since the ferroelectricity in HfO_2-based films has been reported [1], [2], [3], [4], [5], [6], [7], [8], [9], [10], [11], [12]. Hafnia ferroelectric (FE) materials play a crucial role in the operation of FE memory devices, such as FE field effect transistors (FeFETs), FE random access memory (FeRAM), and FE tunnel junctions (FTJs) because of their CMOS compatibility, high scalability, likely 3-D integration, and superior retention [13], [14], [15], [16], [17], [18], [19], [20], [21], [22], [23], [24], [25]. Thus, the key to improve the performance of various FE memory devices lies in a comprehensive understanding of ferroelectricity and the switching behavior of FE materials.

The origin of the FE property derives from the noncentrosymmetric $Pca2_1$ *o*-phase, which is transferred from the *t*-phase owing to the similarities in their structures [26]. Several factors have been reported to affect the FE characteristics of hafnia-based thin films, such as cation and anion doping, oxygen concentration, atomic layer deposition (ALD) deposition temperature, surface and volume effects, stress and strain, and capping electrode [27], [28], [29], [30], [31], [32], [33], [34], [35]. It turns out that the combination of thermodynamic and kinetic variables causes ferroelectricity in fluorite-structured FE material [34], [36]. In particular, according to the FE materials' kinetics, the stabilized *t*-phase during annealing can transfer to the *o*-phase rather than monoclinic (*m*-) phase during cooling process, given that a significant energy barrier ($\Delta E_{t\rightarrow m}$) is formed between the *t*- and *m*-phases [34]. However, due to a high energy barrier between *t*- and *m*-phases during the cooling process, once the *m*-phase

0018-9383 © 2024 IEEE. Personal use is permitted, but republication/redistribution requires IEEE permission. See https://www.ieee.org/publications/rights/index.html for more information.

Authorized licensed use limited to: Korea Advanced Inst of Science & Tech - KAIST. Downloaded on October 25,2024 at 04:42:24 UTC from IEEE Xplore. Restrictions apply.

This article has been accepted for inclusion in a future issue of this journal. Content is final as presented, with the exception of pagination.

is formed, it is unlikely to transition into other metastable phases. The m-phase, which is stable at a rather high temperature, causes a deterioration in the FE characteristics [26]. Consequently, to prevent the unwanted formation of the m-phase, several efforts have been carried out to increase $\Delta E_{t\rightarrow m}$ by introducing the dopant ion Al^{3+}, which has a smaller crystal radius compared to Hf^{4+}, thereby inhibiting the formation of the undesirable m-phase [37]. Kim et al. [38] conducted a study on metal–FE–metal (MFM) capacitors based on HfO_2, where they used Al dopant, finding that the Al:HfO_2 capacitors have a greater energy barrier, $\Delta E_{t\rightarrow m}$, than Zr:$HfO_2$. Additionally, the Al:$HfO_2$ material maintains stable FE characteristics even when subjected to high thermal budget in subsequent processes, owing to its comparatively high crystallization temperature. However, there has been a lack of research so far on determining the most effective annealing technique to both stabilize the FE o-phase and secure uniform domain switching by maximizing the phase transformation from t-phase to o-phase in Al:HfO_2 material.

Recently, several annealing techniques have been proposed to suppress the m-phase formation. Buyantogtokh et al. [39] discovered that high-pressure annealing system reduced the energy barrier between t-phase and o-phase ($\Delta E_{t\rightarrow o}$), while raising the energy barrier between t-phase and m-phase ($\Delta E_{t\rightarrow m}$). Accordingly, the ratio of the o-phase improved as the annealing pressure rose [34]. Moreover, the cooling rate plays a significant part in the transition of t-phase into different phases following crystallization. Toriumi et al. [32] observed that quick ramp-down process could stabilize the FE phase structure. Schroeder et al. [40] found that throughout the cooling process, the high entropy of t-phase brings about a rapid rise in t-phase free energy, which facilitates the transformation from t-phase to either m-phase or o-phase. When the cooling step is finished, the driving force diminishes, resulting in an incomplete transformation from t-phase to the o-phase in the FE thin film. This results in the existence of residual t-phase [41]. Meanwhile, Ku et al. [42] utilized the fast quenching technique to achieve higher P_r and E_C values using a metal–FE–insulator–semiconductor (MFIS) gate-stack. In addition, they further assessed the suitability of the simulation tool for 3-D FE NAND. Nevertheless, there is a lack of experimental research that examines the impact of cooling rates on the polarization, switching speed characteristics, and interfacial quality in hafnia-based FE materials.

In this study, we fabricated capacitors with an Al:HfO_2 MFM structure and subjected them to both fast and slow cooling under different annealing temperature conditions (700 °C, 800 °C, and 900 °C). The o-phase formation was facilitated during annealing at high temperatures, while fast cooling hindered the stabilization of the dielectric m-phase. The experimental results were meticulously investigated using a variety of electrical measurements. In addition, the impact of the cooling rate on the behavior of switching between FE domains was verified by using the nucleation-limited switching (NLS) model. The results showed that as the cooling rate increases, the switching of domains becomes more uniform. The fast cooling capacitor annealed at 900 °C resulted in a higher subloop property due to a reduction in oxygen vacancies (V_O). The quality of the interface was evaluated using

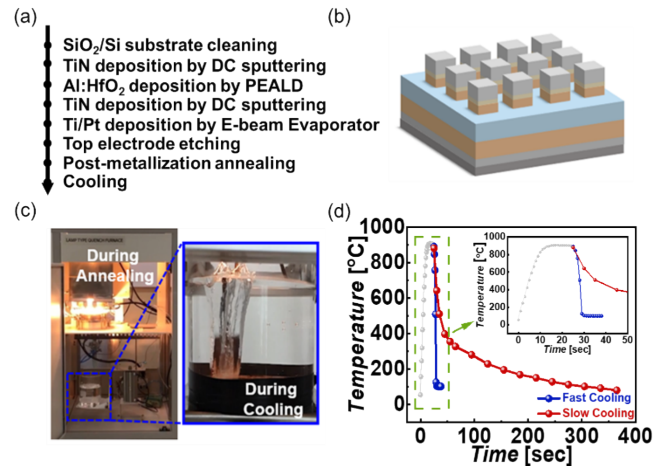

Fig. 1. (a) Process flow of fabricating the Al:HfO_2 MFM structured capacitors. (b) Schematic of MFM capacitor. (c) Customized FRFC system and (d) temperature profiles of fast cooling and slow cooling approaches.

pulse switching measurements, which showed that higher cooling rates lead to increased interfacial capacitance. The findings indicate that fast cooling acts a pivotal part in preventing the creation of the unwanted non-FE dead layer.

II. Experimental Section

We fabricated capacitors with a structure consisting of TiN/Al:HfO_2/TiN in this study. The dc sputtering technique was used to deposit a bottom electrode made of TiN with a thickness of 100 nm, as well as a top electrode made of TiN with a thickness of 50 nm. On the bottom electrode, a layer of Al:HfO_2, with a thickness of 10 nm, was formed at 320 °C by plasma-enhanced ALD (PEALD). The ratio of Hf to Al (29:1) was adjusted by altering the Hf and Al cycle ratios within the supercycle. TEMAHf and TMA were used as precursors to deposit HfO_2 and Al_2O_3 during the Al:HfO_2 deposition process. Oxygen plasma was used for the oxygen reactant. The top electrode was patterned using conventional photolithography and etching processes. Following the fabrication of the MFM capacitor, we performed postmetallization annealing (PMA) at varied temperatures (700 °C, 800 °C, and 900 °C) for 10 s, employing two different cooling rates: fast cooling and slow cooling. Throughout the PMA procedure, we raised the temperature by 50 °C/s in a nitrogen atmosphere. After the annealing procedure, the capacitors that went through fast cooling were subjected to water cooling, whereas the capacitors that performed slow cooling were subjected to chamber cooling in a nitrogen atmosphere. We conducted a variety of electrical analyses using the Keithley 4200 analyzer, including polarization versus electric field (P–E), capacitance versus voltage (C–V), time-dependent polarization switching, and transient switching current.

III. Results and Discussion

Fig. 1(a) and (b) illustrates the fabricating process flow and the schematic of TiN/Al:HfO_2/TiN-structured MFM, respectively. Fig. 1(d) shows the temperature's change over time. The annealing temperature was raised to 900 °C from room temperature at a ramping speed of 50 °C/s, which is similar to

Authorized licensed use limited to: Korea Advanced Inst of Science & Tech - KAIST. Downloaded on October 25,2024 at 04:42:24 UTC from IEEE Xplore. Restrictions apply.

This article has been accepted for inclusion in a future issue of this journal. Content is final as presented, with the exception of pagination.

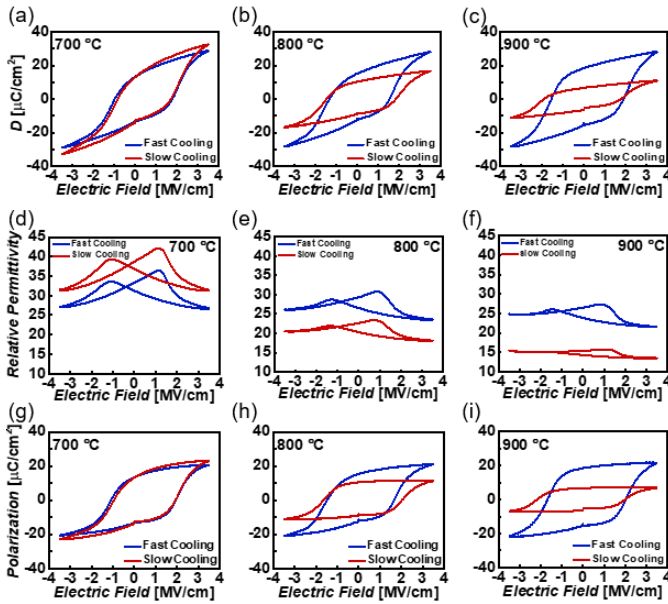

Fig. 2. (a)–(c) D–E curves, (d)–(f) corresponding relative permittivity–electric field curves, and (g)–(i) obtained P–E curves of the capacitors with various annealing temperatures followed by fast cooling and slow cooling techniques.

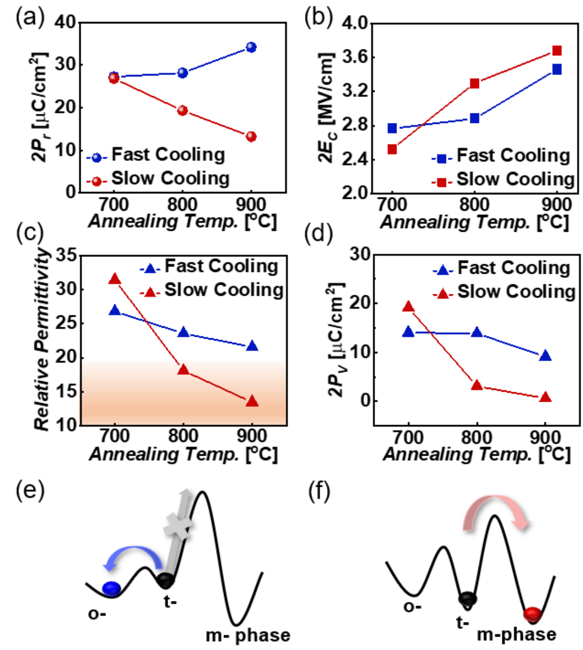

Fig. 3. Comparison of the extracted (a) $2P_r$ values, (b) $2E_C$ values, (c) ε_r values, and (d) $2P_V$ values. Energy landscape of (e) fast cooling and (f) slow cooling.

the conventional rapid temperature annealing (RTA) system. As demonstrated in Fig. 1(c) and (d), after completing the annealing process, for the fast cooling process, the temperature of the sample dropped from 900 °C to room temperature within 5 s in our designed annealing system. In contrast, in the case of the slow cooling process, it took as long as 340 s for the sample temperature to decrease from 900 °C to room temperature.

To analyze the crystalline phase of the Al-doped hafnia FE layer annealed at various temperatures (700 °C, 800 °C, and 900 °C), electrical measurements were performed, and the D–E curves and corresponding relative permittivity–electric field curves of MFM devices after the domain depinning process are shown in Fig. 2(a)–(f). For depinning the domains in $Al:HfO_2$ layer, the D–E curves were acquired after 10^4 cycles of electric switching [43], [44]. The dielectric component contributes to the electric displacement to some extent [43]. Therefore, in order to extract and compare the relative phase fraction within the thin films, it is essential to obtain the P–E curves. We gained the P–E curves, as shown in Fig. 2(g)–(i), by utilizing the D–E and relative permittivity–electric field curves to eliminate the linear dielectric part in the FE thin film according to the following equation [43]:

$$2P = 2D - 2\varepsilon_0\varepsilon_r E \quad (1)$$

where P is a part of D that does not include the dielectric component, D indicates the total displacement, ε_0 means the permittivity of vacuum, and ε_r is the relative permittivity. Moreover, variable polarization (P_V) values that are proportional to the section of the t-phase were extracted with the following equation [38], [43]:

$$2P_V = 2D_{\max} - 2\varepsilon_0\varepsilon_r E_{\max} - 2P_r = 2P_s - 2P_r \quad (2)$$

where $D_{\max}$ is the maximum displacement, $E_{\max}$ means the maximum electric field, which is 3.5 MV/cm in this study, $2P_r$ is the remanent polarization, and $2P_s$ is the saturated polarization. Fig. 3(a)–(d) illustrates the extracted $2P_r$, $2E_C$, ε_r, and $2P_V$ parameters of FE $Al:HfO_2$ films with different annealing temperatures and two types of cooling processes obtained from Fig. 2. The o- and t-phase fractions in the thin films are proportionate to the $2P_r$ and $2P_V$ values, respectively [38]. Additionally, the m-phase fraction can be assessed with the ε_r value. When the ε_r value is smaller than 20, it signifies that the m-phase is dominant [38]. From Fig. 3(d), we observed that as the annealing temperature increased, both the $2P_V$ values for fast cooling and slow cooling decreased, indicating a reduction in the t-phase fraction, suggesting a transformation of the t-phase into other phases. According to Fig. 3(a), in the case of fast cooling, the $2P_r$ values increased with increasing the annealing temperature, indicating a transition of more t-phase into o-phase. In contrast, when the annealing temperature increased, the slow cooling devices exhibited a reduction in $2P_r$ values, suggesting a decrease in the proportion of the o-phase. Especially, the FE layer that has been annealed at high temperatures, 800 °C and 900 °C, followed by slow cooling, shows a significant dominance of the m-phase, as evidenced by the continuous decrease in the ε_r value below 20. This indicates that with increasing annealing temperature, the phase transition from the t-phase to the m-phase became more pronounced rather than transitioning to the o-phase. At an annealing temperature of 700 °C, the $2P_r$ value of the fast cooling capacitor is slightly higher than that of the slow cooling capacitor, indicating a comparable o-phase fraction in both capacitors. For elevated annealing temperatures, 800 °C and 900 °C, the $2P_r$ values of fast cooling were larger than those of slow cooling, implying that fast cooling process prompts a superior o-phase ratio. We measured the maximum $2P_r$ value of about 35.31 $\mu C/cm^2$ and the maximum $2E_C$ value

Authorized licensed use limited to: Korea Advanced Inst of Science & Tech - KAIST. Downloaded on October 25,2024 at 04:42:24 UTC from IEEE Xplore. Restrictions apply.

This article has been accepted for inclusion in a future issue of this journal. Content is final as presented, with the exception of pagination.

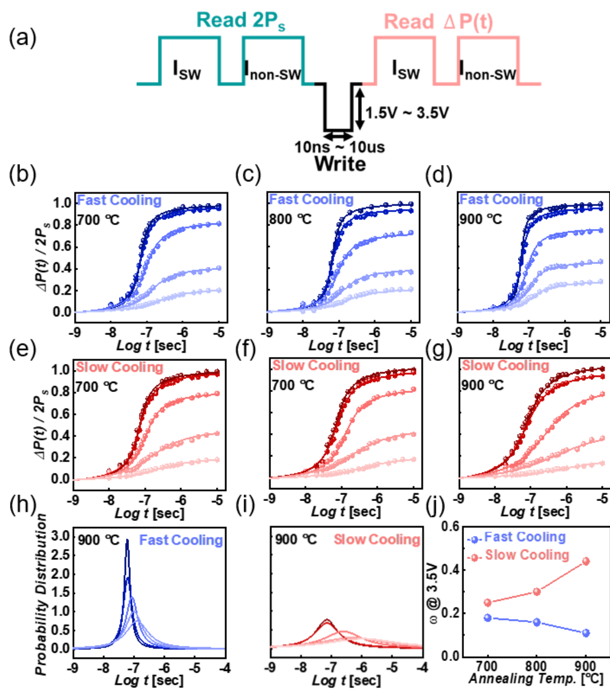

Fig. 4. (a) Pulse profile of $\Delta P(t)/2P_S$ measurement. Time dependent of the polarization change $\Delta P(t)/2P_S$ with relation to various external voltages for (b)–(d) fast cooling and (e)–(g) slow cooling preceded by annealing at 700 °C, 800 °C, and 900 °C. Lorentzian-distribution functions of NLS model for the capacitors annealed at the temperature of 900 °C with (h) fast cooling and (i) slow cooling. (j) Comparison of ω values at the external voltage of 3.5 V versus annealing temperature.

of approximately 3.53 MV/cm when the annealing temperature reached to 900 °C. These values are important determinants of the memory window for FeFET devices. These results suggest that the phase transition during cooling process is significantly influenced by the cooling rate. As the cooling rate increases, the transition from t-phase to m-phase is inhibited, as seen in Fig. 3(e) [40]. Compared with fast cooling, as the FE layer is exposed to high temperature and subjected to slow cooling, the phase transition from t-phase to m-phase becomes significant within the FE layer, and once stabilized, the m-phase is irreversible [Fig. 3(f)] [36]. These findings indicate that fast cooling can suppress the transition from t-phase to m-phase effectively, particularly at high annealing temperatures. Additionally, it can boost the fraction of the desirable o-phase as a result.

To gain a deeper understanding of the switching behavior of the Al-doped hafnia FE layer, we used the NLS model to analyze the polarization switching behavior within domains, which is governed by nucleation [29], [45], [46]. The NLS model characterizes the switching dynamics in polycrystalline thin films. In this model, the waiting time required for nucleation determines the domain switching time [39]. As depicted in Fig. 4(a), two positive 10-μs read pulses to obtain $2P_S$ was applied, followed by a negative writing pulse. The $2P_S$ comprises a switching pulse and a nonswitching pulse. In order to determine the polarization changes over time, $\Delta P(t)$, we employed two positive read pulses lasting 10 μs each, following the application of a negative write pulse with different magnitudes ranging from 1.5 to 3.5 V and widths varying from 10 ns to 10 μs. In addition, (3) was used to fit the $\Delta P(t)/2P_S$ data using the NLS model. The NLS model incorporates a Lorentzian-distribution function that describes the domain switching times in the logarithmic domain

$$\frac{\Delta P(t)}{2P_S} = \int_{-\infty}^{\infty}\left[1-\exp\left\{-\left(\frac{t}{t_0}\right)^2\right\}\right]F(\log t_0)d(\log t_0) \quad (3)$$

where

$$F(\log t_0) = \frac{A}{\pi}\left[\frac{\omega}{(\log t_0 - \log t_1)^2+\omega^2}\right] \quad (4)$$

where A is a constant of normalization, ω means the half-width at half-maximum, and log t_1 values represent the median logarithmic value of the distribution [47]. Fig. 4(b)–(g) displays the $\Delta P(t)/2P_S$ values of the Al:HfO_2 capacitors that undergo annealing at temperatures of 700 °C, 800 °C, and 900 °C using two different cooling methods (fast cooling and slow cooling). The external voltage applied ranged from 1.5 to 3.5 V. The solid lines depict the data that has been adjusted to meet the NLS model. Fig. 4(h) and (i) displays the Lorentzian-distribution functions, determined by fitting the results of annealing at a temperature of 900 °C, using (4).

Fig. 4(j) illustrates the obtained ω values under the application of a voltage of 3.5 V. When the rate of change of $\Delta P(t)/2P_S$ is greater, the ω value is smaller, and the distribution is sharper, indicating a more uniform switching of HfO_2 domains [38], [48]. Devices subjected to fast cooling exhibit lower ω values, indicating more uniform domain switching of the FE film due to the suppression of m-phase transformation and the maximization of the o-phase. The increase in ω values with rising annealing temperatures under slow cooling conditions may be attributed to the decrease in the fraction of the o-phase and the gradual degradation of interface quality, both of which disrupt uniform domain switching [50]. Remarkably, this inclination aligns with the outcomes of the $2P_r$ values and ε_r values depicted in Fig. 3(a) and (c). Furthermore, the subloop characteristics of Al:HfO_2 thin films were investigated by subjecting them to voltage pulses ranging from 0.5 to 3.5 MV/cm, with increments of 0.2 MV/cm, and a rise and fall time of 10 μs. Fig. 5(a) and (b) displays the D–E hysteresis loops of the devices annealed at 900 °C, with fast cooling and slow cooling, respectively. Fig. 5(c) depicts the displacement that has been normalized. Polarization switching was seen in devices with slow cooling at relatively low voltages, displaying nonuniform domain switching. It was observed that the fast cooling process could suppress the subloops at low electric fields. This is crucial for applications, such as FeRAM, which require uniform high polarization at low voltages [50]. Additionally, it can be utilized to applications like FE-NAND, where disturbances are prevented below certain voltages as there is no polarization; whereas polarization occurs only above a specific voltage, enabling PGM or ERS operations [51].

It has been reported that V_O is responsible for the formation of pinned domains, which in turn leads to nonuniform domain switching in slow cooling devices, as depicted in Fig. 5(d) [38], [45]. The fast cooling samples displayed a

Authorized licensed use limited to: Korea Advanced Inst of Science & Tech - KAIST. Downloaded on October 25,2024 at 04:42:24 UTC from IEEE Xplore. Restrictions apply.

This article has been accepted for inclusion in a future issue of this journal. Content is final as presented, with the exception of pagination.

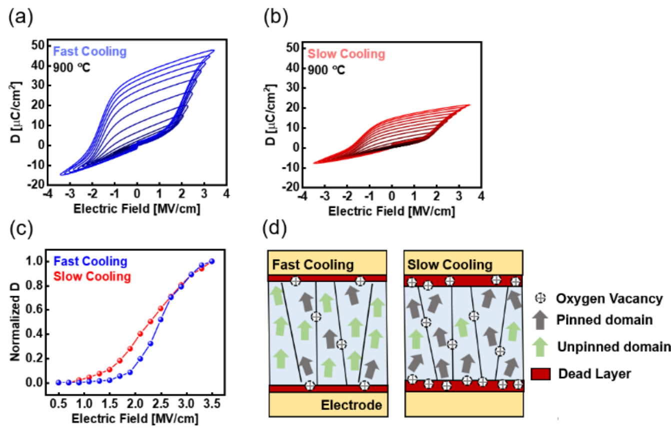

Fig. 5. *D–E* hysteresis loops of (a) fast cooling and (b) slow cooling devices annealed at 900 °C. (c) Normalized displacement. (d) Schematic of domain pinning stemming from the oxygen vacancies of fast cooling and slow cooling devices.

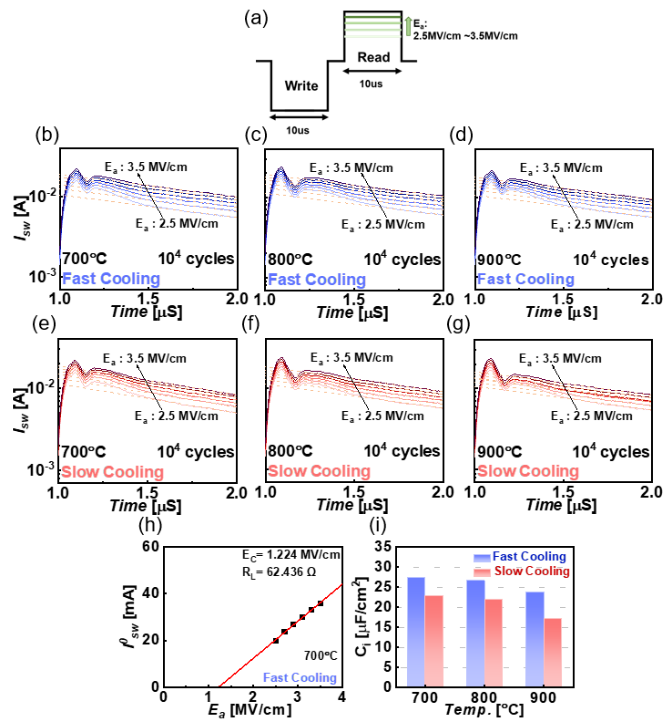

Fig. 6. (a) Pulse sequence of pulse switching measurement. (b)–(g) Transient switching current–time curves of capacitors with various annealing temperatures (700 °C, 800 °C, and 900 °C) for fast cooling and slow cooling. (h) Starting switching current (I^0_{sw}) in relation to the applied electric field (E_a) for the device annealed at 700 °C followed by fast cooling. Comparison of the extracted (i) interfacial dead layer capacitance (C_i) values with respect to annealing temperature.

smaller ω value and uniform switching, reflected by the results in Figs. 4(h) and (j) and 5(c). These observations suggest a lower concentration of V_O in the Al:HfO_2 thin films treated with fast cooling. It is hypothesized that V_O is created by removing oxygen from Al:HfO_2 during the ALD deposition or annealing process [53]. Hence, in order to comprehensively investigate the non-FE layer of the capacitors, the C_i values were quantitatively calculated to assess the development of V_O by pulse-switching experiments. According to the pulse sequence in Fig. 6(a), an initial prepolarization of the films in the up direction was used using a negative write pulse (3.5 MV/cm and 10 μs). Subsequently, a series of positive read pulses with different electric fields ranging from 2.5 to 3.5 MV/cm were used. In order to provide efficient field effect switching, even when the electric field strength is 2.5 MV/cm, the pulse widths of 10 μs were maintained. The switching transient current (I_{SW}) was analyzed in relation to time, as seen in Fig. 6(b)–(g). In the following equation describes the switching transient current, I_{SW}, at a specific electric field, E, according to the reverse domain nucleation and growth model for FE domain switching [54]:

$$I_{SW}(t) = I^0_{SW} e^{-\frac{t-t_0}{R_L C_i}} (t_0 \le t \le t_{SW}) \quad (5)$$

where I^0_{SW} is the current when FE switching starts, C_i is the interfacial dead layer capacitance, R_L indicates the entire resistance of the measuring system and the device, and t_0 and t_{SW} are the time at which the FE film switching begins and completes, respectively. According to Fig. 6(b)–(g), the capacitance charging is represented by an increased I_{SW} at the beginning of the pulse application, which is subsequently succeeded by a decreased current with time as the charging is finished. When t equals t_0, which means that FE polarization switches, $I_{SW}(t)$ follows (5) and complies with the linear behavior for the log-scale (y-axis) represented as yellow dotted lines. I^0_{SW}, which means the current at the beginning of the switching, is described by the following equation:

$$I^0_{SW} = \frac{(E_a - E_c)t_f}{R_L} \quad (6)$$

where E_a represents the applied electric field, and t_f means the thickness of Al:HfO_2 layer. Exactly, E_C indicates the electric field across the FE film, and the remaining fraction of the E_a drops across both the non-FE layer and the load resistance as the polarization begins to switch. By fitting this linear region of I_{SW} using (5), I^0_{SW} and $R_L C_i$ can be acquired. More specifically, with (5), R_L and E_C is extracted by plotting I^0_{SW} as a function of E_a, and then, E_C and the time constant (τ) can be obtained through the x-intercept and slope of the plotting results. As the product of R_L and C_i is τ, C_i can be calculated by dividing τ by R_L. It could be observed that the E_C values gained here are smaller than the E_C values extracted from the P–E curves. This can be interpreted by the extra voltage applied to the non-FE layer and the load resistance. Fig. 6(h) depicts the graph of I^0_{SW} versus E_a for the fast cooling device annealed at 700 °C. The interfacial capacitance arises from an inherent TiO_xN_y or TiO_2 layer generated during the ALD process or annealing process [55]. A greater C_i value suggests a reduced effective thickness of the non-FE layer. According to the results presented in Fig. 6(i), the C_i values obtained from fast cooling are higher than those obtained from slow cooling, suggesting that it effectively prevents the formation of the interface dead layer between the electrode and FE film [56]. This phenomenon can be attributed to a lower level of oxidation of the top TiN and bottom TiN electrodes induced by fast cooling, resulting in less formation of TiO_xN_y or TiO_2, as well as a reduction in V_O. Additionally, the disparity in the C_i values between the two distinct cooling rates consistently demonstrates an

Authorized licensed use limited to: Korea Advanced Inst of Science & Tech - KAIST. Downloaded on October 25,2024 at 04:42:24 UTC from IEEE Xplore. Restrictions apply.

This article has been accepted for inclusion in a future issue of this journal. Content is final as presented, with the exception of pagination.

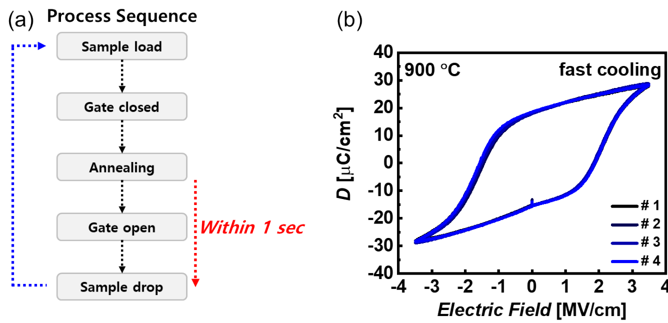

Fig. 7. (a) Detailed process sequence of FRFC annealing. (b) *D–E* curves of the four Al-doped HfO_2 MFM-structured capacitors after annealing at 900 °C followed by fast cooling.

upward trend with increasing the annealing temperature. This suggests that both the top TiN and bottom TiN electrodes are more oxidized due to the severe thermal budget during slow cooling, forming a thicker dead layer where no FE switching takes place [52]. The interfacial dead layer after slow cooling leads to the polarization pinning effect, which disrupts uniform domain switching. These findings indicate that fast cooling can improve the quality of interfaces, allowing for uniform domain switching.

Finally, Fig. 7(a) illustrates the detailed process sequence of the fast ramping fast cooling (FRFC) process. In this system, after annealing, the chamber gate automatically opens, and the sample loader is immersed into the coolant. This entire process occurs within 1 s. Such a system enables a reproducible and reliable FRFC process. Fig. 7(b) shows the *D–E* curves of MFM capacitors subjected to the same FRFC process across four different lots. We believe that this FRFC process represents a starting point for the development of new processes applicable to high-performance, next-generation devices that require high-quality FEs.

IV. Conclusion

To examine the impact of cooling rate on the FE properties of thin films, we fabricated Al:HfO_2 capacitors with a Hf:Al ratio of 29:1 in MFM structures. The capacitors were subsequently annealed at various temperatures using two distinct cooling techniques: fast cooling and slow cooling. We systematically verified the influence of the cooling rate through a range of electrical analyses. The phase analysis tool was employed to identify the phase fraction in the FE materials. Annealing at 900 °C followed by fast cooling resulted in a maximum remanent polarization ($2P_r$) of approximately 35.31 $\mu C/cm^2$. The influence of cooling rate on the polarization switching behavior was studied by employing the NLS model. The results indicated that a fast cooling procedure can lead to more uniform domain switching, diminishing the disturb issues in memory devices. Measurements were performed to determine the portion of the non-FE dead layer through transient pulse switching. The findings suggest that fast cooling is advantageous in preventing the formation of a dead layer, leading to improved interface quality and decreased amount of V_O. The fast cooling process is essential for the maximization of desired *o*-phase, suppression of the unwanted *m*-phase, and inhibition of the interfacial dead layer, thus achieving uniform domain switching. This study not only demonstrates the impact of the fast cooling process on the formation of the FE phase in FE thin films but also holds significance as a potential starting point for future research on cooling processes.

References

[1] H. Joh, M. Jung, J. Hwang, Y. Goh, T. Jung, and S. Jeon, “Flexible ferroelectric hafnia-based synaptic transistor by focused-microwave annealing,” *ACS Appl. Mater. Interfaces*, vol. 14, no. 1, pp. 1326–1333, Jan. 2022.

[2] V. Gaddam, G. Kim, T. Kim, M. Jung, C. Kim, and S. Jeon, “Novel approach to high κ (∼59) and low EOT (∼3.8 Å) near the morphotropic phase boundary with AFE/FE (ZrO_2/HZO) bilayer heterostructures and high-pressure annealing,” *ACS Appl. Mater. Interfaces*, vol. 14, no. 38, pp. 43463–43473, Sep. 2022.

[3] J. Lee et al., “Role of oxygen vacancies in ferroelectric or resistive switching hafnium oxide,” *Nano Converg.*, vol. 10, no. 1, p. 55, Dec. 2023.

[4] M. Kobayashi, J. Wu, Y. Sawabe, S. Takuya, and T. Hiramoto, “Mesoscopic-scale grain formation in HfO_2-based ferroelectric thin films and its impact on electrical characteristics,” *Nano Converg.*, vol. 9, no. 1, p. 50, Nov. 2022.

[5] J. Hwang, H. Joh, C. Kim, J. Ahn, and S. Jeon, “Monolithically integrated complementary ferroelectric FET XNOR synapse for the binary neural network,” *ACS Appl. Mater. Interface*, vol. 16, no. 2, pp. 2467–2476, Jan. 2024.

[6] H. Shin et al., “A method of controlling the imprint effect in Hafnia ferroelectric device,” *Appl. Phys. Lett.*, vol. 122, no. 2, Jan. 2023, Art. no. 022901.

[7] T. S. Böscke, J. Müller, D. Bräuhaus, U. Schröder, and U. Böttger, “Ferroelectricity in hafnium oxide thin films,” *Appl. Phys. Lett.*, vol. 99, no. 10, Sep. 2011, Art. no. 102903.

[8] M. H. Park et al., “Ferroelectricity and antiferroelectricity of doped thin HfO_2-based films,” *Adv. Mater.*, vol. 27, no. 11, pp. 1811–1831, 2015.

[9] U. Schroeder et al., “Impact of different dopants on the switching properties of ferroelectric hafniumoxide,” *Jpn. J. Appl. Phys.*, vol. 53, no. 8S1, Jul. 2014, Art. no. 08LE02.

[10] S. Mueller et al., “Incipient ferroelectricity in Al-doped HfO_2 thin films,” *Adv. Funct. Mater.*, vol. 22, no. 11, pp. 2412–2417, Mar. 2012.

[11] S. Mueller, C. Adelmann, A. Singh, S. V. Elshocht, U. Schroeder, and T. Mikolajick, “Ferroelectricity in Gd-doped HfO_2 thin films,” *ECS J. Solid State Sci. Technol.*, vol. 1, no. 6, Oct. 2012, Art. no. N123.

[12] J. Müller et al., “Ferroelectric hafnium oxide: A CMOS-compatible and highly scalable approach to future ferroelectric memories,” in *IEDM Tech. Dig.*, Dec. 2013, pp. 10.8.1–10.8.4.

[13] G. Kim et al., “Power-delay area-efficient processing-in-memory based on nanocrystalline Hafnia ferroelectric field-effect transistors,” *ACS Appl. Mater. Interfaces*, vol. 15, no. 1, pp. 1463–1474, Jan. 2023.

[14] H. Mulaosmanovic, E. T. Breyer, T. Mikolajick, and S. Slesazeck, “Ferroelectric FETs with 20-nm-Thick HfO_2 layer for large memory window and high performance,” *IEEE Trans. Electron Devices*, vol. 66, no. 9, pp. 3828–3833, Sep. 2019.

[15] M. H. Park, Y. H. Lee, T. Mikolajick, U. Schroeder, and C. S. Hwang, “Review and perspective on ferroelectric HfO_2-based thin films for memory applications,” *MRS Commun.*, vol. 8, no. 3, pp. 795–808, Sep. 2018.

[16] Z. Fan, J. Chen, and J. Wang, “Ferroelectric HfO_2-based materials for next-generation ferroelectric memories,” *J. Adv. Dielectrics*, vol. 6, no. 2, Jun. 2016, Art. no. 1630003.

[17] T. S. Böscke, J. Müller, D. Bräuhaus, U. Schröder, and U. Böttger, “Ferroelectricity in hafnium oxide: CMOS compatible ferroelectric field effect transistors,” in *IEDM Tech. Dig.*, Dec. 2011, pp. 24.5.1–24.5.4.

[18] S. Lee et al., “Effect of floating gate insertion on the analog states of ferroelectric field-effect transistors,” *IEEE Trans. Electron Devices*, vol. 70, no. 1, pp. 349–353, Jan. 2023.

[19] S. Lee, G. Kim, T. Kim, T. Eom, and S. Jeon, “Vertical-pillar ferroelectric field-effect-transistor memory,” *Phys. Status Solidi (RRL) Rapid Res. Lett.*, vol. 16, no. 10, Oct. 2022, Art. no. 2100532.

[20] Y. Goh et al., “High performance and self-rectifying hafnia-based ferroelectric tunnel junction for neuromorphic computing and TCAM applications,” in *IEDM Tech. Dig.*, Dec. 2021, pp. 17.2.1–17.2.4.

Authorized licensed use limited to: Korea Advanced Inst of Science & Tech - KAIST. Downloaded on October 25,2024 at 04:42:24 UTC from IEEE Xplore. Restrictions apply.

This article has been accepted for inclusion in a future issue of this journal. Content is final as presented, with the exception of pagination.

[21] V. Garcia and M. Bibes, "Ferroelectric tunnel junctions for information storage and processing," *Nature Commun.*, vol. 5, no. 1, Jul. 2014, Art. no. 4289.

[22] C. Yoon, S. Moon, and C. Shin, "Study of a hysteresis window of FinFET and fully-depleted silicon-on-insulator (FDSOI) MOSFET with ferroelectric capacitor," *Nano Converg.*, vol. 7, no. 1, pp. 1–7, Jun. 2020.

[23] H. K. Yoo et al., "Engineering of ferroelectric switching speed in Si doped HfO_2 for high-speed 1T-FERAM application," in *IEDM Tech. Dig.*, Dec. 2017, p. 19.

[24] M. Jung, V. Gaddam, and S. Jeon, "A review on morphotropic phase boundary in fluorite-structure Hafnia towards DRAM technology," *Nano Converg.*, vol. 9, no. 1, pp. 1–18, Oct. 2022.

[25] M. Hellenbrand and J. MacManus-Driscoll, "Multi-level resistive switching in hafnium-oxide-based devices for neuromorphic computing," *Nano Converg.*, vol. 10, no. 1, p. 44, Sep. 2023.

[26] M. H. Park, H. J. Kim, Y. J. Kim, W. Lee, T. Moon, and C. S. Hwang, "Evolution of phases and ferroelectric properties of thin $Hf_{0.5}Zr_{0.5}O_2$ films according to the thickness and annealing temperature," *Appl. Phys. Lett.*, vol. 102, no. 24, Jun. 2013, Art. no. 242905.

[27] U. Schroeder, C. S. Hwang, and H. Funakubo, *Ferroelectricity in Doped Hafnium Oxide: Materials, Properties and Devices*. Sawston, U.K.: Woodhead Publishing, 2019.

[28] R. Batra, T. D. Huan, G. A. Rossetti, and R. Ramprasad, "Dopants promoting ferroelectricity in hafnia: Insights from a comprehensive chemical space exploration," *Chem. Mater.*, vol. 29, no. 21, pp. 9102–9109, Nov. 2017.

[29] T.-H. Ryu, D.-H. Min, and S.-M. Yoon, "Comparative studies on ferroelectric switching kinetics of sputtered $Hf_{0.5}Zr_{0.5}O_2$ thin films with variations in film thickness and crystallinity," *J. Appl. Phys.*, vol. 128, no. 7, Aug. 2020, Art. no. 074102.

[30] M. Materano, P. D. Lomenzo, A. Kersch, M. H. Park, T. Mikolajick, and U. Schroeder, "Interplay between oxygen defects and dopants: Effect on structure and performance of HfO_2-based ferroelectrics," *Inorganic Chem. Frontiers*, vol. 8, no. 10, pp. 2650–2672, 2021.

[31] K. D. Kim et al., "Ferroelectricity in undoped-HfO_2 thin films induced by deposition temperature control during atomic layer deposition," *J. Mater. Chem. C*, vol. 4, no. 28, pp. 6864–6872, 2016.

[32] A. Toriumi et al., "Material perspectives of HfO_2-based ferroelectric films for device applications," in *IEDM Tech. Dig.*, Dec. 2019, pp. 15.1.1–15.1.4.

[33] H. A. Hsain et al., "Many routes to ferroelectric HfO_2: A review of current deposition methods," *J. Vac. Sci. Technol. A, Vac. Surf. Films*, vol. 40, no. 1, Dec. 2021, Art. no. 010803.

[34] M. H. Park et al., "Understanding the formation of the metastable ferroelectric phase in hafnia–zirconia solid solution thin films," *Nanoscale*, vol. 10, no. 2, pp. 716–725, 2018.

[35] S. J. Kim et al., "Large ferroelectric polarization of TiN/$Hf_{0.5}Zr_{0.5}O_2$/TiN capacitors due to stress-induced crystallization at low thermal budget," *Appl. Phys. Lett.*, vol. 111, no. 24, Dec. 2017, Art. no. 242901.

[36] M. H. Park, Y. H. Lee, T. Mikolajick, U. Schroeder, and C. S. Hwang, "Thermodynamic and kinetic origins of ferroelectricity in fluorite structure oxides," *Adv. Electron. Mater.*, vol. 5, no. 3, Mar. 2019, Art. no. 1800522.

[37] R. D. Shannon, "Revised effective ionic radii and systematic studies of interatomic distances in halides and chalcogenides," *Acta Crystallographica Sect. A*, vol. 32, no. 5, pp. 751–767, Sep. 1976.

[38] G. Kim et al., "Design guidelines of thermally stable Hafnia ferroelectrics for the fabrication of 3D memory devices," in *IEDM Tech. Dig.*, Dec. 2022, pp. 5.4.1–5.4.4.

[39] B. Buyantogtokh, V. Gaddam, and S. Jeon, "Effect of high pressure anneal on switching dynamics of ferroelectric hafnium zirconium oxide capacitors," *J. Appl. Phys.*, vol. 129, no. 24, Jun. 2021, Art. no. 244106.

[40] U. Schroeder, M. H. Park, T. Mikolajick, and C. S. Hwang, "The fundamentals and applications of ferroelectric HfO_2," *Nature Rev. Mater.*, vol. 7, no. 8, pp. 653–669, Mar. 2022.

[41] Y. Zheng et al., "In-situ atomic-level observation of reversible first-order transition in $Hf_{0.5}Zr_{0.5}$ O_2 ferroelectric film," in *IEDM Tech. Dig.*, Dec. 2022, pp. 6.3.1–6.3.4.

[42] B. Ku, S. Choi, Y. Song, and C. Choi, "Fast thermal quenching on the ferroelectric Al: HfO_2 thin film with record polarization density and flash memory application," in *Proc. IEEE Symp. VLSI Technol.*, Jun. 2020, pp. 1–2.

[43] M. H. Park et al., "Effect of Zr content on the wake-up effect in $Hf_{1-x}Zr_xO_2$ films," *ACS Appl. Mater. Interface*, vol. 8, no. 24, pp. 15466–15475, Jun. 2016.

[44] J. Müller et al., "Ferroelectricity in simple binary ZrO_2 and HfO_2," *Nano Lett.*, vol. 12, no. 8, pp. 4318–4323, Aug. 2012.

[45] W. Wei et al., "In-depth understanding of polarization switching kinetics in polycrystalline $\mathbf{Hf}_{0.5}\mathbf{Zr}_{0.5}\mathbf{O}_2$ ferroelectric thin film: A transition from NLS to KAI," in *IEDM Tech. Dig.*, Dec. 2021, p. 19.

[46] A. K. Tagantsev, I. Stolichnov, N. Setter, J. S. Cross, and M. Tsukada, "Non-Kolmogorov-Avrami switching kinetics in ferroelectric thin films," *Phys. Rev. B, Condens. Matter*, vol. 66, no. 21, Dec. 2002, Art. no. 214109.

[47] J. Y. Jo, H. S. Han, J.-G. Yoon, T. K. Song, S.-H. Kim, and T. W. Noh, "Domain switching kinetics in disordered ferroelectric thin films," *Phys. Rev. Lett.*, vol. 99, no. 26, Dec. 2007, Art. no. 267602.

[48] T. Y. Lee et al., "Ferroelectric polarization-switching dynamics and wake-up effect in Si-doped HfO_2," *ACS Appl. Mater. Interface*, vol. 11, no. 3, pp. 3142–3149, Jan. 2019.

[49] F. Mehmood et al., "Bulk depolarization fields as a major contributor to the ferroelectric reliability performance in lanthanum doped $Hf_{0.5}Zr_{0.5}O_2$ capacitors," *Adv. Mater. Interface*, vol. 6, no. 21, Nov. 2019, Art. no. 1901180.

[50] S.-C. Chang et al., "FeRAM using anti-ferroelectric capacitors for high-speed and high-density embedded memory," in *IEDM Tech. Dig.*, Dec. 2021, pp. 33.2.1–33.2.4.

[51] M.-K. Kim, I.-J. Kim, and J.-S. Lee, "CMOS-compatible ferroelectric NAND flash memory for high-density, low-power, and high-speed three-dimensional memory," *Sci. Adv.*, vol. 7, no. 3, Jan. 2021, Art. no. eabe1341.

[52] Y. Goh, S. H. Cho, S.-H. K. Park, and S. Jeon, "Oxygen vacancy control as a strategy to achieve highly reliable Hafnia ferroelectrics using oxide electrode," *Nanoscale*, vol. 12, no. 16, pp. 9024–9031, 2020.

[53] M. Pešić et al., "Physical mechanisms behind the field-cycling behavior of HfO_2-based ferroelectric capacitors," *Adv. Funct. Mater.*, vol. 26, no. 25, pp. 4601–4612, 2016.

[54] H. J. Kim et al., "A study on the wake-up effect of ferroelectric $Hf_{0.5}Zr_{0.5}O_2$ films by pulse-switching measurement," *Nanoscale*, vol. 8, no. 3, pp. 1383–1389, 2016.

[55] D. Das, B. Buyantogtokh, V. Gaddam, and S. Jeon, "Influence of high-pressure annealing conditions on ferroelectric and interfacial properties of Zr-rich $Hf_xzr_{1-x}O_2$ capacitors," *IEEE Trans. Electron Devices*, vol. 68, no. 4, pp. 1996–2002, Apr. 2021.

[56] S. Yun et al., "Effect of annealing temperature on minimum domain size of ferroelectric Hafnia," 2023, *arXiv:2301.05374*.

Authorized licensed use limited to: Korea Advanced Inst of Science & Tech - KAIST. Downloaded on October 25,2024 at 04:42:24 UTC from IEEE Xplore. Restrictions apply.